A crucial role of CeO2–ZrO2 support for the low temperature water gas shift reaction over Cu–CeO2–ZrO2 catalysts

ARTICLE *in* CATALYSIS SCIENCE & TECHNOLOGY · MAY 2015

Impact Factor: 5.43 · DOI: 10.1039/C5CY00499C

5 AUTHORS, INCLUDING:

Dae-Woon Jeong
University of Toronto
43 PUBLICATIONS **441** CITATIONS
SEE PROFILE

Jae-Oh Shim
Yonsei University
27 PUBLICATIONS **221** CITATIONS
SEE PROFILE

Won-Jun Jang
Yonsei University
33 PUBLICATIONS **233** CITATIONS
SEE PROFILE

Hyun-Seog Roh
Yonsei University
127 PUBLICATIONS **2,938** CITATIONS
SEE PROFILE

Catalysis Science & Technology

PAPER

View Article Online
View Journal

Cite this: DOI: 10.1039/c5cy00499c

A crucial role for the CeO_2–ZrO_2 support for the low temperature water gas shift reaction over Cu–CeO_2–ZrO_2 catalysts†

Dae-Woon Jeong, Hyun-Suk Na, Jae-Oh Shim, Won-Jun Jang and Hyun-Seog Roh*

Received 3rd April 2015,
Accepted 11th May 2015

DOI: 10.1039/c5cy00499c

www.rsc.org/catalysis

A co-precipitation method was employed to prepare Cu dispersed on CeO_2, ZrO_2 and CeO_2–ZrO_2 supports to obtain catalysts useful for the low temperature water gas shift (WGS) reaction. To optimize the Cu–CeO_2–ZrO_2 catalysts, the CeO_2/ZrO_2 ratio was systematically changed. The cubic phase Cu–$Ce_{0.8}Zr_{0.2}O_2$ catalyst exhibited the highest turnover frequency and the lowest activation energy among the catalysts tested and its CO conversion was maintained without significant loss during the reaction for 100 h. The enhanced catalytic activity and stability of the co-precipitated Cu–$Ce_{0.8}Zr_{0.2}O_2$ was mainly attributed to an enhanced oxygen mobility and a strong resistance against the sintering of Cu, resulting from a large amount of defect oxygen and the strong interaction between CuO and cubic phase $Ce_{0.8}Zr_{0.2}O_2$.

Introduction

Interest in the water gas shift (WGS) reaction has recently been renewed because of its use in fuel processors for small-scale reformers.[1] A conventional WGS process comprises a high temperature WGS (350–450 °C) and a low temperature WGS (180–250 °C). However, commercial WGS catalysts (Fe_2O_3–Cr_2O_3 catalyst and CuO–ZnO–Al_2O_3 catalyst) cannot be used in small-scale reformers because of restrictions related to volume, weight, and cost. Furthermore, the WGS reaction is a mildly exothermic reaction whose CO conversion is thermodynamically limited at high temperatures.[2,3] For this reason, it is useful to employ the low temperature WGS reaction for small-scale reformers. Consequently, the challenge with low temperature WGS is to develop catalysts which are sufficiently active (hydrogen production per unit hour), and have high long-term stability.

Among the various metal-based catalysts examined in the literature, Cu-based catalysts are promising candidates for the low temperature WGS reaction. Metallic Cu is generally accepted to exhibit a good CO oxidation and H_2O dissociative adsorption capacity and the cost of Cu is lower than that of noble metals.[4–6] A Cu–Zn–Al catalyst has been used for the low temperature WGS reaction in commercial plants; however this catalyst is not suitable for use in a small-scale reformer because of its pyrophoric nature, susceptibility to chemical poisoning, and slow kinetics.[4,7–12] Therefore, the development of Cu-based catalysts for the low temperature WGS reaction has been the subject of ongoing interest for many research groups.[4–6,13–15]

In the case of CeO_2 support, the facile $Ce^{4+} \leftrightarrow Ce^{3+}$ redox cycle often leads to a higher oxygen storage capacity (OSC), where the addition and removal of oxygen to/from the fluorite structure of CeO_2 is reversible. Much effort has been focused on the direct doping of metal ions (Al, Zr, Hr, Si, and La) into the lattice of CeO_2. Redox properties better than those of CeO_2 alone can be obtained by the incorporation of metal ions into the CeO_2 lattice, which leads to $Ce_{(1-x)}M_{(x)}O_y$ solid solutions.[16] Additionally, the incorporation of a cation enhances the chemical and physical properties by creating oxygen vacancies inside the parent oxide. In particular, the introduction of ZrO_2 into the CeO_2 lattice is known to significantly enhance the classical behavior of CeO_2 by increasing its high thermal resistance and excellent OSC.[5,17–24] Therefore, the CeO_2–ZrO_2 system is a promising candidate for use as a support material in the WGS reaction at low temperature.

Only a limited number of studies have been concerned with this objective. To our knowledge, Cu–CeO_2 catalysts showed the best performance among Cu-based catalysts for WGS in the literature. Pradhan *et al.* reported that a Cu–CeO_2–ZrO_2 catalyst achieved the equilibrium CO conversion at 350 °C and at a GHSV of 5000 h^{-1} and it exhibited higher catalytic activity than Cu–CeO_2 catalyst.[21] However, its high activity was only observed at a low GHSV and under the

Department of Environmental Engineering, Yonsei University, 1 Yonseidae-gil, Wonju, Gangwon 220-710, South Korea. E-mail: hsroh@yonsei.ac.kr; Fax: +82 33 760 2571

† Electronic supplementary information (ESI) available: H_2 consumption of the Cu–CeO_2, Cu–ZrO_2, and Cu–CeO_2–ZrO_2 catalysts. See DOI: 10.1039/c5cy00499c

diluted reaction conditions, specifically, when the reactants were diluted with N_2 (35–50% N_2 in reactant gases).

We have previously reported that a co-precipitated Cu–CeO_2 catalyst achieved almost equilibrium CO conversion at an extremely high GHSV of 36 076 h^{-1}.[4] Jiang *et al.* reported that a Cu–CeO_2–ZrO_2 catalyst exhibited higher catalytic activity/stability than Cu–CeO_2 catalyst for the high temperature WGS reaction using a coal-derived synthesis gas.[5] It has been reported that the addition of ZrO_2 to CeO_2 leads to improvements in oxygen storage capacity of CeO_2, redox property, thermal stability, and promotion of metal dispersion due to the partial substitution of Ce^{4+} with Zr^{4+} in the lattice of CeO_2 resulting in solid solution formation.[18,19] From this result, many researchers have concerned that the addition of ZrO_2 into the CeO_2 lattice to increase the activity and stability of Cu-based catalysts for the WGS at low temperature.[4,5,21]

Recently, we designed Cu doped CeO_2–ZrO_2 catalysts with different structures which have been applied for the low temperature WGS reaction to understand the effect of cubic/tetragonal structure of CeO_2–ZrO_2 supports.[25] We also found that the factors correlated with catalytic performance in the low temperature WGS such as reduction property and oxygen mobility strongly depend on the structure of CeO_2–ZrO_2 supports.[25] Although CeO_2, ZrO_2, and CeO_2–ZrO_2 supported Cu catalysts show great promise as WGS catalysts, their properties have not been systemically studied.

The objective of this work is to compare the activity/stability of CeO_2, ZrO_2, and CeO_2–ZrO_2 supported Cu catalysts in the low temperature WGS reaction. Co-precipitated Cu–CeO_2, Cu–ZrO_2, and Cu–CeO_2–ZrO_2 catalysts with various CeO_2/ZrO_2 ratios were prepared and applied to the WGS reaction using a simulated reformate gas at a very high GHSV of 72 152 h^{-1}. It will be useful to evaluate activity/stability of Cu–CeO_2–ZrO_2 catalysts by employing ceria–zirconia supports having either cubic structure (CeO_2 rich composition) or tetragonal structure (ZrO_2 rich composition) in low temperature WGS. The effects of the CeO_2/ZrO_2 ratios on the properties of the CeO_2–ZrO_2 were evaluated by BET, N_2O-chemisorption, X-ray diffraction (XRD), temperature programmed reduction (TPR), and X-ray photoelectron spectroscopy (XPS). The catalyst characteristics were also correlated to their catalytic performance (CO conversion, turnover frequency, and activation energy) in the low temperature WGS.

Experimental

Catalyst preparation

Cu–CeO_2–ZrO_2 mixed oxide catalysts with various CeO_2/ZrO_2 ratios were prepared by a one step co-precipitation/digestion method. The loading amount of Cu was fixed at 20 wt%. Compositions containing 80, 60, 40, and 20 equivalent mol% of CeO_2 are referred to as Cu–$Ce_{0.8}Zr_{0.2}O_2$, Cu–$Ce_{0.6}Zr_{0.4}O_2$, Cu–$Ce_{0.4}Zr_{0.6}O_2$, and Cu–$Ce_{0.2}Zr_{0.8}O_2$ respectively. Stoichiometric quantities of $Cu(NO_3)_3{\cdot}xH_2O$ (99%, Aldrich), $Ce(NO_3)_3{\circ}6H_2O$ (99%, Aldrich) and a zirconyl nitrate solution (20 wt% ZrO_2 basis, MEL Chemicals) were dissolved in distilled water. A 15 wt% KOH solution was added drop-wise to the previous solution at 80 °C with constant stirring to attain a pH of 10.5. The precipitates were aged at 80 °C for 3 days. They were subsequently washed five times with distilled water, air-dried for 24 h, and then dried at 110 °C for 6 h. The Cu–CeO_2 and Cu–ZrO_2 catalysts were also prepared according to the same procedure. The catalysts were calcined at 400 °C for 6 h.

Characterization

The BET surface area was measured by nitrogen adsorption at −196 °C using an ASAP 2010 (Micromeritics). XRD patterns were recorded using a Rigaku D/MAX-IIIC diffractometer (Ni filtered Cu–Kα radiation, 40 kV, 50 mA). Temperature-programmed reduction (TPR) experiments were carried out in an Autochem 2910 (Micromeritics). The detailed procedure for TPR was described in the previous paper.[26,27] N_2O-chemisorption was conducted in an Autochem II 2920 (Micromeritics). Prior to the N_2O-chemisorption, the fresh samples were reduced at 250 °C for 2 h with 10 vol% H_2/Ar. The consumption of N_2O and the release of N_2 on the metallic Cu sites ($N_2O + 2Cu = Cu_2O + N_2$) were measured at 60 °C by a thermal conductivity detector (TCD). XPS spectra were obtained using a Kα spectrophotometer (Themo-Scientific), with a high resolution monochromator. The pressure of the analysis chamber was kept at 6.8×10^{-9} mbar and was kept working with the detector in constant energy mode with pass energy of 100 eV for the survey spectrum and 50 eV for the detailed scan. The binding energy was calibrated using the C 1s transition, appearing at 284.6 eV.

Water gas shift reaction test unit

The WGS reactions were conducted in a micro-tubular quartz reactor at a fixed pressure of 1 atm, and the reaction temperature was varied from 200 to 400 °C. Details regarding the WGS reaction have been previously reported in the literature.[28] The simulated reformed gas consisted of 6.5 vol% CO, 7.1 vol% CO_2, 0.7 vol% CH_4, 42.4 vol% H_2, 28.7 vol% H_2O, and 14.5 vol% N_2, which represents a typical reformed gas from a fuel processor. The feed $H_2O/(CH_4 + CO + CO_2)$ ratio was intentionally fixed at 2.0 because the H_2O/CH_4 ratio is typically 3.0 in SRM to avoid the formation of coke. The criteria used to evaluate the performance of the reaction are shown below.

$$\text{CO conversion}(\%) = \frac{1 - [\text{CO}]_{\text{out}} / [\text{CO}]_{\text{in}}}{1 + [\text{CO}]_{\text{out}}} \times 100$$

$$\text{CO}_2\ \text{selectivity}(\%) = \frac{[\text{CO}_2]_{\text{out}} - [\text{CO}_2]_{\text{in}}}{\left([\text{CH}_4]_{\text{out}} - [\text{CH}_4]_{\text{in}}\right) + \left([\text{CO}_2]_{\text{out}} - [\text{CO}_2]_{\text{in}}\right)} \times 100$$

where $[CO]_{in}$ and $[CO]_{out}$ are the inlet and outlet concentrations of CO.

Measurements of turnover frequency (TOF) were obtained in separate experiments where the conversion of CO was kept below 20% so that differential reaction conditions could be assumed with negligible heat and mass-transfer effects. TOF was calculated using the following equation,

$$\mathrm{TOF}\left(\mathrm{s}^{-1}\right)=\frac{\left([\mathrm{CO}]_{\mathrm{in}}-[\mathrm{CO}]_{\mathrm{out}}\right)\times \mathrm{AB}_{M}\times F}{D\times W\times X_{\mathrm{M}}}$$

where $[CO]_{in}$ and $[CO]_{out}$ are the inlet and outlet concentrations of CO, AB_M is the atomic weight of metal M, F is the total flow rate (mol s^{-1}), D is the metal dispersion, W is the mass of catalyst (g), and X_M the metal content (g_{metal}/g_{cat}), respectively.

The Arrhenius plot can be obtained from the relation between TOF and temperature using the following formula,

$$y=-\frac{E_{\mathrm{a}}}{R}x+\ln A$$

where y is the TOF, x is the reciprocal of the absolute temperature, R is the universal gas constant, and E_a is activation energy. The E_a can be calculated from the slope of the fitted Arrhenius plot.

Results and discussion

Catalyst characterization

Characteristics of co-precipitated Cu–CeO_2, Cu–ZrO_2, and Cu–CeO_2–ZrO_2 catalysts are given in Table 1. With increasing Zr content, the BET surface area increased. The value of the BET surface area varied from 119.3 to 272.3 $m^2\ g^{-1}$, with the Cu–ZrO_2 catalyst exhibiting the highest value (272.3 $m^2\ g^{-1}$). On the contrary, the change in the dispersion of Cu in the Cu–CeO_2, Cu–ZrO_2, and Cu–CeO_2–ZrO_2 catalysts followed the reverse trend of the BET surface area. The Cu dispersion values ranged from 3.5 to 8.5%, with the Cu–CeO_2 catalyst exhibiting the highest value (8.5%). As a result, the Cu–CeO_2 catalyst possessed the smallest Cu particle size among the prepared catalysts. The addition of Zr clearly led to an increase in the BET surface area and the Cu particle size and to diminished Cu dispersion. It should be noted that BET surface area of Cu–$Ce_{0.2}Zr_{0.8}O_2$ is much higher than that of Cu–$Ce_{0.8}Zr_{0.2}O_2$ but the Cu particle size of the Cu–$Ce_{0.8}Zr_{0.2}O_2$ is smaller than that of the Cu–$Ce_{0.2}Zr_{0.8}O_2$ catalyst. Likewise, the Cu dispersion of Cu–$Ce_{0.8}Zr_{0.2}O_2$ is higher than that of Cu–$Ce_{0.2}Zr_{0.8}O_2$ even though the BET surface area of the former is less than the value of the latter. This indicates that $Ce_{0.8}Zr_{0.2}O_2$ support helps to achieve a higher Cu dispersion.

Table 1 Characteristics of Cu–CeO_2, Cu–ZrO_2, and Cu–CeO_2–ZrO_2 catalysts

Catalyst	Catalyst S.A. ($m^2\ g^{-1}$)[a]	Cu dispersion (%)[b]	Cu particle size (nm)[b]
Cu–CeO_2	119.3	8.5	11.8
Cu–$Ce_{0.8}Zr_{0.2}O_2$	155.7	7.8	12.9
Cu–$Ce_{0.6}Zr_{0.4}O_2$	205.0	6.8	14.8
Cu–$Ce_{0.4}Zr_{0.6}O_2$	233.8	5.8	17.3
Cu–$Ce_{0.2}Zr_{0.8}O_2$	246.0	5.6	17.9
Cu–ZrO_2	272.3	3.5	28.6

[a] Estimated from N_2 adsorption at −196 °C. [b] Estimated from N_2O-chemisorption.

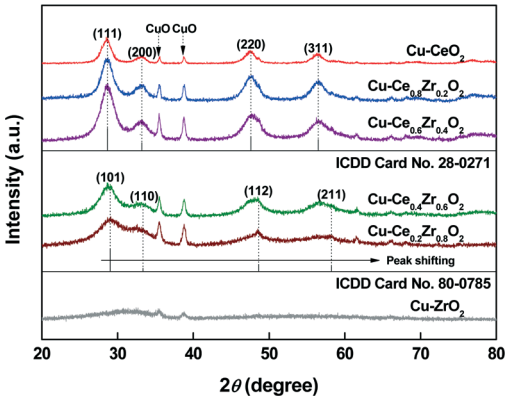

Fig. 1 XRD patterns of Cu–CeO_2, Cu–ZrO_2, and Cu–CeO_2–ZrO_2 catalysts.

XRD patterns for the Cu–CeO_2, Cu–ZrO_2, and Cu–CeO_2–ZrO_2 catalysts are given in Fig. 1. Peaks associated with cubic CeO_2 and CuO were observed in the XRD pattern of the Cu–CeO_2 catalyst. The XRD patterns of the Cu–CeO_2–ZrO_2 catalysts shifted to higher angles compared to those of the Cu–CeO_2 catalyst. This shift is mainly related to a change in the lattice parameters and indicates that Zr^{4+} (0.84 Å), with a smaller ionic radius than Ce^{4+} (0.97 Å), was inserted into the CeO_2 lattice.[18,19] The Ce^{4+} ion has an eight-coordination of oxygen ions.[5] The unit cell contains four cations locating the opposite corners.[5] Thus, Ce^{4+} ions can be replaced by Zr^{4+}.[5] As a result, a solid solution was formed for CeO_2–ZrO_2 support.

Oxygen vacancies were also generated in the CeO_2–ZrO_2 solid solution by tetravalent Ce^{4+} cation, and these vacancies are profitable in redox reactions.[5] In the redox mechanism, carbon monoxide is adsorbed on the metal and is oxidized at the metal/oxide interface with the formation of carbon dioxide.[29] The oxygen vacancy on the surface is then re-oxidized by water. This fact indicates that the oxygen vacancy of the support plays a vital role in controlling the activity/stability of the catalyst during WGS. Therefore, the CeO_2–ZrO_2 solid solution supported Cu catalyst was expected to have a beneficial effect on the WGS activity.[5] Like CeO_2, the Cu–$Ce_{0.8}Zr_{0.2}O_2$ and Cu–$Ce_{0.6}Zr_{0.4}O_2$ catalysts exhibited cubic structure (ICDD card no. 28–0271), whereas the Cu–$Ce_{0.4}Zr_{0.6}O_2$ and Cu–$Ce_{0.2}Zr_{0.8}O_2$ catalysts exhibited a tetragonal structure (ICDD card no. 80–0785).[18] This result is consistent with the report that 25 mol% ZrO_2 or more is sufficient to obtain a tetragonal phase in ceria–zirconia solid solution.[30] In the case of the Cu–ZrO_2 catalyst, XRD pattern indicated an amorphous structure.[5,20]

The chemical species present on the catalyst surfaces and their proportions were evaluated by XPS. Fig. 2(a) shows the

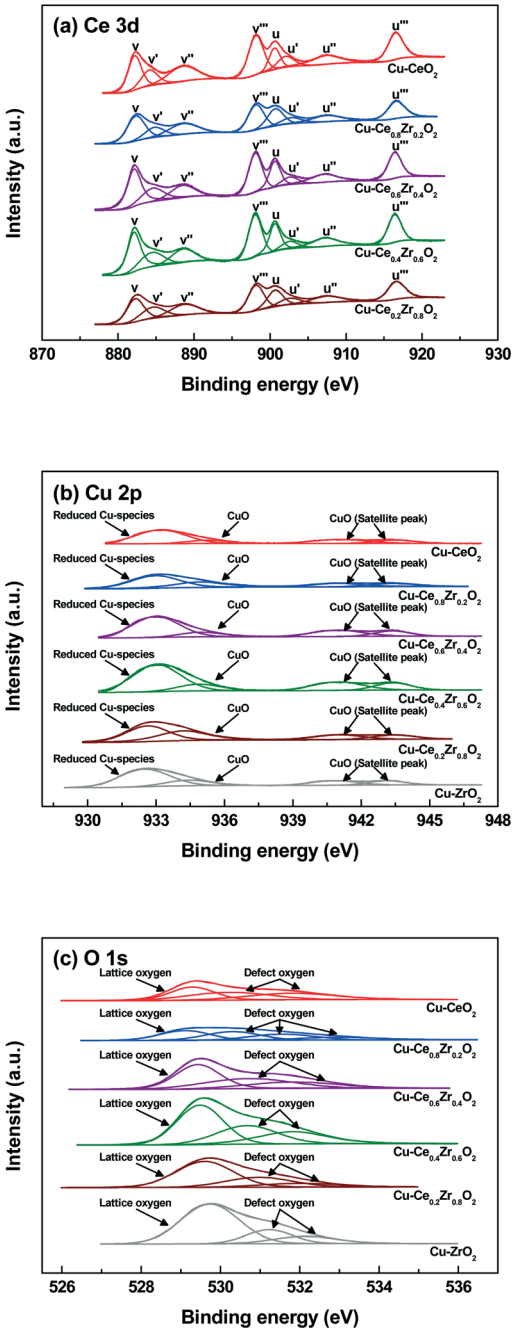

Fig. 2 XPS spectra of Cu–CeO_2, Cu–ZrO_2, and Cu–CeO_2–ZrO_2 catalysts: (a) Ce 3d, (b) Cu 2p, and (c) O 1s.

Ce 3d spectra of all the CeO_2 supported catalysts prepared in this study. The curves of the Ce 3d spectra in the prepared catalysts are composed of eight peaks corresponding to four pairs of spin-orbit doublets. The main Ce $3d_{5/2}$ peaks located at 882.3, 884.8, 888.5 and 898.1 eV assigned to *v*, *v*′, *v*″ and *v*‴ components, while the four peaks of Ce $3d_{3/2}$ centered at 900.6, 902.7, 907.4 and 916.6 eV assigned to *u*, *u*′, *u*″, and *u*‴ components, respectively.[25] The main peaks marked by *v*, *v*″, *v*‴, *u*, *u*″ and *u*‴ are correspond to the $3d^{10}4f^0$ state of Ce^{4+} ions, whereas those denoted by *v*′ and *u*′ are attributed to the $3d^{10}4f^1$ electronic state of the Ce^{3+} ions. These peaks indicated that

Table 2 Surface atomic ratio estimated by XPS

	Cu species (%)		Ce species	O species (%)	
Catalyst	CuO	Reduced Cu	Ce^{3+}/Ce^{4+}	Lattice O	Defect O
Cu–CeO_2	40	60	0.19	33	67
Cu–$Ce_{0.8}Zr_{0.2}O_2$	36	64	0.20	30	70
Cu–$Ce_{0.6}Zr_{0.4}O_2$	42	58	0.18	44	56
Cu–$Ce_{0.4}Zr_{0.6}O_2$	43	57	0.18	47	53
Cu–$Ce_{0.2}Zr_{0.8}O_2$	44	56	0.17	60	40
Cu–ZrO_2	41	59	—	68	32

cerium co-existed as Ce^{4+} and Ce^{3+}. The ratio of Ce^{3+}/Ce^{4+} was calculated by measuring the area of the corresponding peaks and the results are shown in Table 2. Cu–$Ce_{0.8}Zr_{0.2}O_2$ showed the highest Ce^{3+}/Ce^{4+} ratio among the tested catalysts. The Ce^{3+}/Ce^{4+} ratio of Cu–CeO_2–ZrO_2 catalysts are decreased with increasing Zr contents (>20%). This is mainly due to the irreducible property of ZrO_2. It should be noted that Cu–$Ce_{0.8}Zr_{0.2}O_2$ exhibited the highest Ce^{3+}/Ce^{4+} ratio, which represents the dominance of Ce^{3+} as compared to others. It has been established that the formation of Ce^{3+} ions accompanied by defect oxygen on a ceria surface. Thus, it is expected that this catalyst should have the largest amount of defect oxygen.

Fig. 2(b) depicts the Cu $2p_{3/2}$ spectra of CeO_2, ZrO_2 and CeO_2–ZrO_2 supported Cu catalysts. A broad peak was observed in the range of 930–938 eV indicative of the presence of various copper species. The satellite peaks at 940–945 eV can be assigned to the presence of CuO in all the catalysts. The wide Cu $2p_{3/2}$ spectra of the prepared catalysts were deconvoluted in two components as shown in Fig. 2(b). The predominant peak at 932.6–933 eV is assigned to the reduced Cu species. The small peak at 934.1–935 eV is due to Cu^{2+} species of CuO based on reported literature data.[31] It should be noted that Cu–$Ce_{0.8}Zr_{0.2}O_2$ catalyst has higher concentration of reduced Cu species than others (Table 2). It is well known that the reduced copper species play as a catalytically active species in WGS reaction.[32] Thus, higher concentration of reduced copper species in Cu–$Ce_{0.8}Zr_{0.2}O_2$ catalyst is expected to show higher activity in WGS reaction. On the other hand, the increase of Zr addition (>20%) in ceria resulted in the decrease of reduced copper species.

The O 1s spectra of the CeO_2, ZrO_2 and CeO_2–ZrO_2 supported Cu catalysts show a broad peak and can be resolved by deconvolution (Fig. 2(c)). The peak at 529.0–529.5 eV is due to the lattice oxygen present in the metal oxides while other peaks are assigned to the defect oxygen.[33] Defect oxygen corresponds to the mobile oxygen ions such as O^{2-}, O^- or adsorbed oxygen species from hydroxyl or water species on the surface.[34] The lattice oxygen gradually shifted to the higher binding energy with increasing the Zr amount, which might be due to higher binding energy of the lattice oxygen in ZrO_2 than in CeO_2. Interestingly, the amount of defect oxygen also decreases with increase of the Zr loadings. This is mainly due to the formation of bulk ZrO_2. Kašpar and Dutta reported that the doping of Zr^{4+} into CeO_2 could cause structural distortion, resulting in the generation of labile oxygen

or weak bonding oxygen.[35] Surface defect oxygen has been considered to be the most active oxygen and to play an important role in oxidation reaction. The increase of the defect oxygen can promote the oxidation of CO into CO_2 and initiate the water dissociation, which in turn releases the hydrogen. In addition, the defect oxygen has an important role on dispersion of metal, resulting from the anchoring on the support surface. Therefore, it is expected that cubic Cu–$Ce_{0.8}Zr_{0.2}O_2$ catalyst should have higher activity than others for the WGS reaction due to the high oxygen mobility and Cu dispersion.

Fig. 3 shows the H_2-TPR patterns of the Cu–CeO_2, Cu–ZrO_2, and Cu–CeO_2–ZrO_2 catalysts. The TPR patterns of cubic Cu–CeO_2 showed two reduction peaks at 139 °C and 207 °C. The first broad peak is associated with the reduction of surface CuO species.[36] The second peak is assigned to the reduction of CuO species interacting with the support.[36] Upon the introduction of a relatively small amount of Zr (*i.e.*, Cu–$Ce_{0.8}Zr_{0.2}O_2$), the interaction between CuO and support was enhanced and a peak was observed at a higher temperature of 215 °C. However, in cases where the Zr contents ranged from 20 to 80% in CeO_2–ZrO_2 supports, the main peaks are shifted to lower temperature with increasing Zr contents. The pattern of amorphous Cu–ZrO_2 catalyst showed a reduction peak at 186 °C. This peak was assigned to the reduction of the CuO species with an interaction with the ZrO_2.[13] Notably, the CuO species interacting with the support of cubic Cu–$Ce_{0.8}Zr_{0.2}O_2$ catalyst can be reduced at the highest temperature. This result indicated that the cubic Cu–$Ce_{0.8}Zr_{0.2}O_2$ catalyst possessed the strong interaction between CuO and support. The sintering phenomenon is well known to be inhibited by the strong interaction between a metal and its support.[6,14] According to the recent literature, a strong resistance to Cu sintering is important for WGS activity.[6] The H_2 consumption of the Cu–CeO_2, Cu–ZrO_2, and Cu–CeO_2–ZrO_2 catalysts are shown in supporting information (Table S1). In the case of Cu–$Ce_{0.8}Zr_{0.2}O_2$, the total H_2 consumption (4.33 mmol g^{-1}) is higher than the sum of the theoretical value of 2.50 mmol g^{-1} (attributable to the reduction of CuO alone) and *ca.* 1.68 μmol g^{-1} from the surface oxygen in pure ceria. The difference is possibly due to the reduction of ceria sub-layers in the presence of CuO_x interacting with the CeO_2.[12] This result is supported by the largest amount of defect oxygen of Cu–$Ce_{0.8}Zr_{0.2}O_2$ catalyst. Likewise, the calculated H_2 consumption of Cu–CeO_2 and Cu–CeO_2–ZrO_2 is clearly higher than the theoretical H_2 consumption value, which is in good agreement with XPS analysis. On the other hand, Cu–ZrO_2 shows the lowest value of H_2 consumption among the prepared catalysts. Thus, it is expected that the cubic Cu–$Ce_{0.8}Zr_{0.2}O_2$ catalyst should show high activity and stability for the WGS.

Reaction results

To develop a high performance catalyst for the WGS reaction, we tested prepared catalysts at a GHSV of 72 152 h^{-1}, which is 24 times higher than that of the typical WGS experimental conditions. In Fig. 4, the CO conversion rate and CH_4 & CO_2 selectivity are plotted as a function of the reaction temperature for the WGS reaction over the Cu–CeO_2, Cu–ZrO_2, and Cu–CeO_2–ZrO_2 catalysts. Clearly, the activity of the cubic Cu–$Ce_{0.8}Zr_{0.2}O_2$ catalyst was better than that of the other catalysts from 200 to 400 °C. The cubic catalysts exhibited a higher CO conversion than the tetragonal catalysts throughout the entire temperature range. The amorphous Cu–ZrO_2 catalyst exhibited a CO conversion slightly higher than that of the tetragonal Cu–$Ce_{0.2}Zr_{0.8}O_2$ catalyst in the lower part of the temperature range (up to 280 °C). The Cu–$Ce_{0.2}Zr_{0.8}O_2$ catalyst exhibited a higher CO conversion than the Cu–ZrO_2 catalyst at or above 320 °C. The amorphous Cu–ZrO_2 catalyst exhibited the lowest activity, despite the strong interaction between CuO and support, possibly because of the large particle size of Cu. CO_2 selectivity of 100% was achieved with all of the catalysts, indicating that all the catalysts can selectively convert CO into CO_2 without a methanation reaction. Consequently, the Cu–$Ce_{0.8}Zr_{0.2}O_2$ catalyst exhibited the highest CO conversion among the prepared catalysts, as well as 100% CO_2 selectivity.

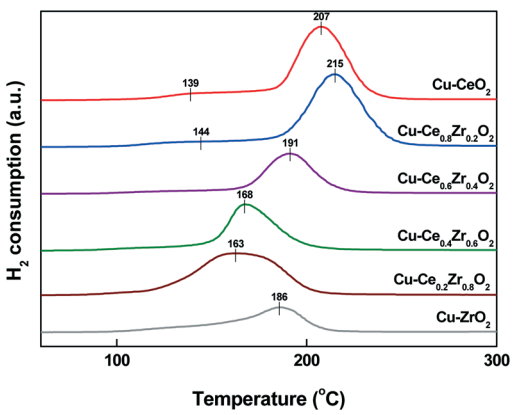

Fig. 3 TPR patterns of Cu–CeO_2, Cu–ZrO_2, and Cu–CeO_2–ZrO_2 catalysts.

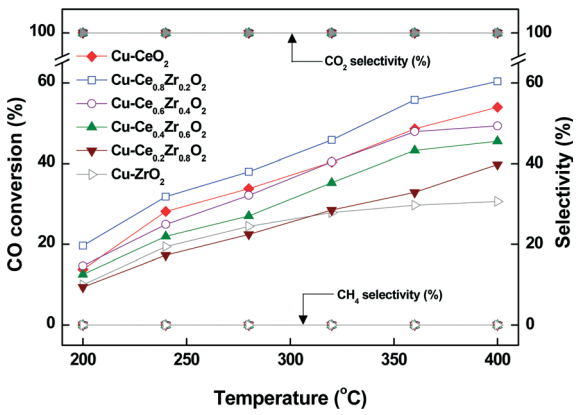

Fig. 4 Conversion and selectivity with reaction temperature over Cu–CeO_2, Cu–ZrO_2, and Cu–CeO_2–ZrO_2 catalysts (H_2O/(CH_4 + CO + CO_2) = 2.0; GHSV = 72 152 h^{-1}).

Table 3 Turnover frequency and activation energy results with reaction temperature over $Cu–CeO_2$, $Cu–ZrO_2$, and $Cu–CeO_2–ZrO_2$ catalysts

Catalyst	Turnover frequency (s^{-1}) 225 °C	230 °C	E_a (kJ mol^{-1})
$Cu–CeO_2$	0.136	0.154	36 ± 1
$Cu–Ce_{0.8}Zr_{0.2}O_2$	0.224	0.247	34 ± 2
$Cu–Ce_{0.6}Zr_{0.4}O_2$	0.104	0.119	40 ± 1
$Cu–Ce_{0.4}Zr_{0.6}O_2$	0.101	0.106	41 ± 1
$Cu–Ce_{0.2}Zr_{0.8}O_2$	0.050	0.056	44 ± 1
$Cu–ZrO_2$	0.054	0.063	52 ± 1

The TOF results are summarized in Table 3. The TOF results were calculated from separate kinetic measurements that were obtained under differential GHSV (150 494 h^{-1}), and they took into account the results of the N_2O-chemisorption experiments.[6,37] The TOF results measured at 225 °C decreased in the following sequence: $Cu–Ce_{0.8}Zr_{0.2}O_2$ (0.224 s^{-1}) > $Cu–CeO_2$ (0.136 s^{-1}) > $Cu–Ce_{0.6}Zr_{0.4}O_2$ (0.104 s^{-1}) > $Cu–Ce_{0.4}Zr_{0.6}O_2$ (0.101 s^{-1}) > $Cu–ZrO_2$ (0.054 s^{-1}) > $Cu–Ce_{0.2}Zr_{0.8}O_2$ (0.050 s^{-1}). At 230 °C, the $Cu–Ce_{0.8}Zr_{0.2}O_2$ catalyst also exhibited the highest TOF value among the prepared catalysts. This result was consistent with the CO conversion and XPS results.

The TOF results are summarized in the Arrhenius-type diagram in Fig. 5, where the TOFs obtained from the examined catalysts were plotted as functions of the reaction temperature. The activation energies (E_a) of the WGS reactions over the $Cu–CeO_2$, $Cu–ZrO_2$, and $Cu–CeO_2–ZrO_2$ catalysts were calculated from the slopes of the fitted lines in Fig. 5. The calculated activation energies are summarized in Table 3. The activation energy increased with increasing Zr content in the $Cu–CeO_2–ZrO_2$ catalysts (the activation energies ranged from 34 ± 2 to 44 ± 1 kJ mol^{-1}). Un-substituted CeO_2 and ZrO_2 supported Cu catalysts exhibited activation energies of 36 ± 1 and 52 ± 1 kJ mol^{-1}, respectively. The $Cu–Ce_{0.8}Zr_{0.2}O_2$ catalyst exhibited the lowest activation energy of 34 ± 2 kJ mol^{-1}. It is interesting to note that the highest CO conversion of the $Cu–Ce_{0.8}Zr_{0.2}O_2$ catalyst is correlated to its lowest activation energy. Thus, it can be proposed that the role of the $Ce_{0.8}Zr_{0.2}O_2$ is to lower the barrier for oxygen transfer from support to the metal, thereby facilitating oxidation of adsorbed CO.

To verify the stability of the prepared catalysts, a long-term WGS reaction test was performed at 320 °C and at a very high GHSV of 72 152 h^{-1} for 100 h (Fig. 6). Interestingly, the $Cu–Ce_{0.8}Zr_{0.2}O_2$ catalyst exhibited very stable catalytic performance, without detectable deactivation of the catalyst (X_{CO} > 40% at 320 °C for 100 h). This result indicates that the stability of Cu based catalysts improved with an increase of Zr contents up to 20%, but further increase of Zr contents resulted in decreased stability. In other words, the other catalysts deactivated fairly rapidly with time on stream. This result matched well with the TPR patterns. The catalyst deactivation of this catalyst is possibly from Cu sintering, the over reduction of a support, and carbon formation. As a result, the $Cu–Ce_{0.8}Zr_{0.2}O_2$ catalyst exhibited high WGS activity as well as a high degree of stability, which is attributed to the strong interaction between CuO and support.

The excellent catalytic performance of the $Cu–Ce_{0.8}Zr_{0.2}O_2$ catalyst can be explained as follows. First, the defect oxygen is an important factor for the WGS reaction. XPS results show that the amount of defect oxygen in cubic $Ce_{0.8}Zr_{0.2}O_2$ catalyst was the highest among the prepared catalysts. The conductivities of defect oxygen through the lattice lead to the formation of oxygen vacancies. The existence of oxygen vacancy in the catalyst is important for the metal dispersion as well as to stabilize copper nanoparticles loaded on support against sintering. Further, the increase of defect oxygen helps to improve oxygen mobility at the surface on the support.[38] The cubic $Ce_{0.8}Zr_{0.2}O_2$ support can give mobile oxygen to oxidize CO to CO_2 by temporarily reducing $Ce^{4+} \leftrightarrow Ce^{3+}$, and then is re-oxidized by taking oxygen from the H_2O molecule.[19,39] As a result, cubic $Cu–Ce_{0.8}Zr_{0.2}O_2$ catalyst showed the highest turnover frequency and the lowest activation energy in the low temperature WGS reaction.

Second, the strong interaction between CuO and support is effective in preventing sintering of Cu. The $Cu–Ce_{0.8}Zr_{0.2}O_2$ catalyst can be reduced at 215 °C, which is the highest

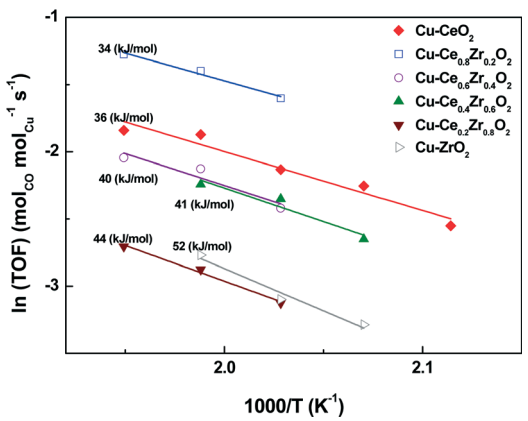

Fig. 5 Arrhenius plots of turnover frequency of CO conversion obtained over $Cu–CeO_2$, $Cu–ZrO_2$, and $Cu–CeO_2–ZrO_2$ catalysts ($H_2O/(CH_4 + CO + CO_2)$ = 2.0; GHSV = 150 494 h^{-1}).

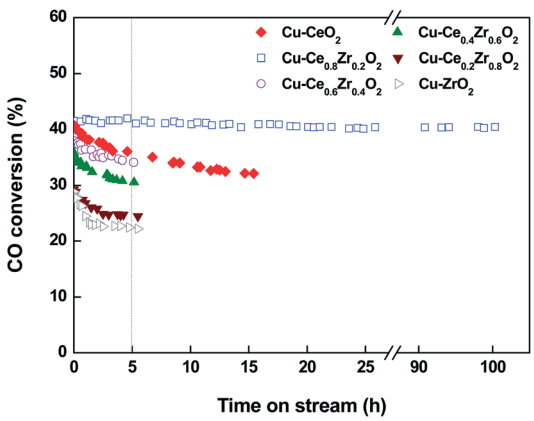

Fig. 6 CO conversion with time on stream over $Cu–CeO_2$, $Cu–ZrO_2$, and $Cu–CeO_2–ZrO_2$ catalysts ($H_2O/(CH_4 + CO + CO_2)$ = 2.0; T = 320 °C; GHSV = 72 152 h^{-1}).

reduction temperature observed in the TPR profiles of the investigated catalysts. In the case of Cu–$Ce_{0.8}Zr_{0.2}O_2$, $Ce_{0.8}Zr_{0.2}O_2$ support acts as the anchors for Cu particles thanks to the strong interaction between CuO and $Ce_{0.8}Zr_{0.2}O_2$. The strong interaction between CuO and $Ce_{0.8}Zr_{0.2}O_2$ support are likely responsible for this catalyst exhibiting the highest thermal stability among the prepared catalysts. As a result, the Cu–$Ce_{0.8}Zr_{0.2}O_2$ catalyst exhibited high activity with good stability even at the extremely high GHSV of 72 152 h^{-1}. Recently, we have also confirmed that a strong resistance to the sintering of Cu is mainly related to the strong interaction between CuO and support.[6]

Third, the Cu dispersion of the catalysts partly affected their catalytic performance. Although the Cu dispersion of the Cu–CeO_2 was higher than that of the Cu–$Ce_{0.8}Zr_{0.2}O_2$ catalyst, the Cu–$Ce_{0.8}Zr_{0.2}O_2$ catalyst exhibited a much higher CO conversion rate compared to that of the Cu–CeO_2 catalyst because of a large amount of defect oxygen. Therefore, the defect oxygen was vastly more important than the Cu dispersion in obtaining high CO conversions in the WGS reaction.

To confirm the above explained relationship, the physicochemical properties and reaction results were compared as shown in Fig. 7. The plotted results match very well with the explained relationship. Fig. 7 (A) shows in agreement with XPS results, that the amount of defect oxygen has a strong effect on the CO conversion and TOF. The trends of TOF and CO conversion are similar to that of amounts of defect oxygen. Thus, it is clearly confirmed that the catalytic activity of Cu based catalysts is correlated to its amount of defect oxygen. To figure out the relation between the thermal stability and the interaction between CuO and support, loss of CO conversion data were collected for 5 h. The calculated loss of CO conversion is in good agreement with the explained TPR profiles, considering the reduction temperature. This strongly indicates that thermal stability of catalyst depends significantly on the strong interaction between CuO and CeO_2–ZrO_2 support. From this fact, it can be concluded that the enhanced catalytic activity and stability of the developed Cu–$Ce_{0.8}Zr_{0.2}O_2$ was mainly attributed to a large amount of defect oxygen and the strong interaction between CuO and $Ce_{0.8}Zr_{0.2}O_2$. On the other hand, we also found that Cu–CeO_2–ZrO_2 with cubic structure helps to achieve a larger amount of defect oxygen and the strong interaction between CuO and support. As a result, cubic Cu–$Ce_{0.8}Zr_{0.2}O_2$ catalyst shows higher activity than tetragonal Cu–$Ce_{0.2}Zr_{0.8}O_2$ catalyst.

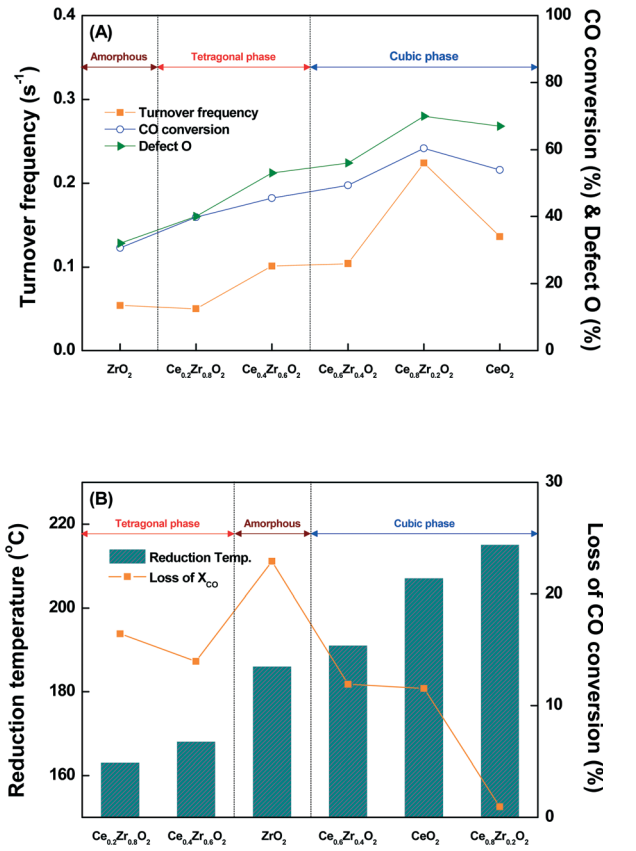

Fig. 7 Relation between the physicochemical properties and reaction results: (A) relation between activity and defect oxygen (B) relation between stability and reduction temperature.

Conclusions

Cu–CeO_2, Cu–ZrO_2, and Cu–CeO_2–ZrO_2 catalysts were prepared by a co-precipitation method and were tested for their feasibility in the low temperature WGS reaction. The Cu–$Ce_{0.8}Zr_{0.2}O_2$ catalyst showed the highest CO conversion among the prepared catalysts with a temperature range from 200 to 400 °C at a very high GHSV of 72 152 h^{-1}. Moreover, the Cu–$Ce_{0.8}Zr_{0.2}O_2$ catalyst exhibited the highest TOF and the lowest activation energy in the low temperature WGS reaction. The high catalytic activity of Cu–$Ce_{0.8}Zr_{0.2}O_2$ catalyst is mainly correlated with the enhanced oxygen mobility, resulting from a large amount of defect oxygen. We also found that the Cu–$Ce_{0.8}Zr_{0.2}O_2$ catalyst exhibited a very stable activity at 320 °C for 100 h. This is due to a strong resistance against Cu sintering, resulting from the strong interaction between CuO and $Ce_{0.8}Zr_{0.2}O_2$ support. Therefore, the Cu–$Ce_{0.8}Zr_{0.2}O_2$ catalyst should be considered as a high-performance catalyst for the low temperature WGS reaction.

Acknowledgements

This research was supported by Basic Science Research Program through the National Research Foundation of Korea (NRF) funded by the Ministry of Science, ICT and Future Planning (2013R1A1A1A05007370).

Notes and references

1 D. L. Trimm and Z. I. Önsan, *Catal. Rev.: Sci. Eng.*, 2001, **43**, 30.
2 H.-S. Roh, H. S. Potdar, D.-W. Jeong, K.-S. Kim, J.-O. Shim, W.-J. Jang, K. Y. Koo and W. L. Yoon, *Catal. Today*, 2012, **185**, 113.
3 R. B. Mane, D.-W. Jeong, A. V. Malawadkar, H.-S. Roh and C. V. Rode, *ChemCatChem*, 2014, **6**, 1698.

4 D.-W. Jeong, W.-J. Jang, J.-O. Shim, W.-B. Han, H.-S. Roh, U. H. Jung and W. L. Yoon, *Renewable Energy*, 2014, **65**, 102.
5 L. Jiang, H. Zhu, R. Razzaq, M. Zhu, C. Li and Z. Li, *Int. J. Hydrogen Energy*, 2012, **37**, 15914.
6 D.-W. Jeong, H.-S. Na, J.-O. Shim, W.-J. Jang, H.-S. Roh, U. H. Jung and W. L. Yoon, *Int. J. Hydrogen Energy*, 2014, **39**, 9135.
7 J. Kugai, J. T. Miller, N. Guo and C. Song, *Appl. Catal., B*, 2011, **105**, 306.
8 J. Kugai, E. B. Fox and C. Song, *Appl. Catal., A*, 2013, **456**, 204.
9 J. A. Rodriguez, J. Evans, J. Graciani, J. B. Park, P. Liu, J. Hrbek and J. F. Sanz, *J. Phys. Chem. C*, 2009, **113**, 7364.
10 J. A. Rodriguez, J. C. Hanson, D. Stacchiola and S. D. Senanayake, *Phys. Chem. Chem. Phys.*, 2013, **15**, 12004.
11 L. Li, Y. Zhan, Q. Zheng, Y. Zheng, C. Chen, Y. She, X. Lin and K. Wei, *Catal. Lett.*, 2009, **130**, 532.
12 H. S. Potdar, D.-W. Jeong, K.-S. Kim and H.-S. Roh, *Catal. Lett.*, 2011, **141**, 1268.
13 J. B. Ko, C. M. Bae, Y. S. Jung and D. H. Kim, *Catal. Lett.*, 2005, **105**, 157.
14 P. Djinović, J. Batista and A. Pintar, *Appl. Catal., A*, 2008, **347**, 23.
15 A. Kubacka, R. Si, P. Michorczyk, A. Martínez-Arias, W. Xu, J. C. Hanson, J. A. Rodriguez and M. Fernández-García, *Appl. Catal., B*, 2013, **132–133**, 423.
16 H. S. Potdar, H.-S. Roh, K. W. Jun, M. Ji and Z.-W. Liu, *Catal. Lett.*, 2002, **84**, 95.
17 D.-W. Jeong, H. S. Potdar, K.-S. Kim and H.-S. Roh, *Bull. Korean Chem. Soc.*, 2011, **32**, 3557.
18 D.-W. Jeong, H. S. Potdar and H.-S. Roh, *Catal. Lett.*, 2012, **142**, 439.
19 D.-W. Jeong, H. S. Potdar, J.-O. Shim, W.-J. Jang and H.-S. Roh, *Int. J. Hydrogen Energy*, 2013, **38**, 4502.
20 H.-S. Roh, I.-H. Eum and D.-W. Jeong, *Renewable Energy*, 2012, **42**, 212.
21 S. Pradhan, A. S. Reddy, R. N. Devi and S. Chilukuri, *Catal. Today*, 2009, **141**, 72.
22 W.-J. Jang, D.-W. Jeong, J.-O. Shim, H.-S. Roh, I. H. Son and S. J. Lee, *Int. J. Hydrogen Energy*, 2013, **38**, 4508.
23 D.-W. Jeong, W.-J. Jang, J.-O. Shim, H.-S. Roh, I. H. Son and S. J. Lee, *Int. J. Hydrogen Energy*, 2013, **38**, 13649.
24 J.-O. Shim, D.-W. Jeong, W.-J. Jang, K.-W. Jeon, B. H. Jeon, S. Y. Cho, H.-S. Roh, J.-G. Na, C. H. Ko, Y.-K. Oh and S. S. Han, *Renewable Energy*, 2014, **65**, 36.
25 D.-W. Jeong, W.-J. Jang, H.-S. Na, J.-O. Shim, A. Jha and H.-S. Roh, *J. Ind. Eng. Chem.*, 2015, DOI: 10.1016/j.jiec.2015.01.007.
26 D.-W. Jeong, V. Subramanian, J.-O. Shim, W.-J. Jang, Y. C. Seo, H.-S. Roh, J. H. Gu and Y. T. Lim, *Catal. Lett.*, 2013, **143**, 438.
27 V. Subramanian, D.-W. Jeong, W.-B. Han, W.-J. Jang, J.-O. Shim and H.-S. Roh, *Int. J. Hydrogen Energy*, 2013, **38**, 8699.
28 T. Bunluesin, R. J. Gorte and G. W. Graham, *Appl. Catal., B*, 1998, **15**, 107.
29 R. O. Fuentes and R. T. Baker, *J. Phys. Chem. C*, 2009, **113**, 914.
30 V. Subramanian, E. S. Gnanakumar, D.-W. Jeong, W.-B. Han, C. S. Gopinath and H.-S. Roh, *Chem. Commun.*, 2013, **49**, 11257.
31 R. B. Mane and C. V. Rode, *Green Chem.*, 2012, **14**, 2780.
32 G. K. Reddy, P. Boolchand and P. G. Smirniotis, *J. Phys. Chem. C*, 2012, **116**, 11019.
33 Q. F. Deng, T. Z. Ren, B. Agula, Y. Liu and Z. Y. Yuan, *J. Ind. Eng. Chem.*, 2014, **20**, 3303.
34 H. Li, G. Lu, Q. Dai, Y. Wang, Y. Guo and Y. Guo, *Appl. Catal., B*, 2011, **102**, 475.
35 B. Shen, Y. Wang, F. Wang and T. Liu, *Chem. Eng. J.*, 2014, **236**, 171.
36 H. Yahiro, K. Murawaki, K. Saiki, T. Yamamoto and H. Yamaura, *Catal. Today*, 2007, **126**, 436.
37 P. Panagiotopoulou and D. I. Kondarides, *J. Catal.*, 2004, **225**, 327.
38 M. Zhao, M. Shen and J. Wang, *J. Catal.*, 2007, **248**, 258.
39 C. Sun, J. Sun, G. Xiao, H. Zhang, X. Qiu, H. Li and L. Chen, *J. Phys. Chem. B*, 2006, **110**, 13445.

